Visible Spectroscopy Measurements in the PBFA II Ion Diode

J. Bailey, A.L. Carlson, and R.L. Morrison

Sandia National Laboratories
Albuquerque, New Mexico, 87185

SAND--90-0631C
DE90 010828

and

Y. Maron
Physics Dept., Weizmann Institute of Science
Rehovot, Israel

Abstract

We describe a new visible spectroscopy diagnostic system for measuring plasma properties in the PBFA II applied-B ion diode. The system transports light from the ion diode to a remote screen room where it is recorded by a spectrograph coupled to a streak camera. We developed extensive calibration techniques for measuring the collection efficiency into the fiber link, the effects of the background bremsstrahlung radiation on the fibers, the fiber transmission as a function of wavelength, and the absolute streaked-spectrograph sensitivity as a function of wavelength. We have recorded time-dependent spectral line profiles and intensities from the PBFA II plasma opening switch, the beam-transport gas cell, and the anode plasma. The Stark shift of the LiI 2s-2p transition observed on LiF-anode shots shows that the time-resolved electric field peaks at 7-8 MV/cm, the highest field ever measured using the Stark effect. The potential of these measurements to expand our knowledge of ion-diode physics is being explored.

I. Introduction

Applied-B ion diodes driven by large pulsed-power accelerators are promising candidates for an inertial-confinement-fusion driver. To achieve the ion beam intensity needed to ignite a thermonuclear target, we must first obtain a detailed understanding of the diode physics. This paper describes methods developed for visible spectroscopy measurements in an applied-B ion diode on the Particle Beam Fusion Accelerator II (PBFA II). This effort has been motivated by the pioneering work using visible spectroscopy on low-power diodes described in References 1-12. A particularly complete set of spectroscopic measurements was obtained by Maron et.al.[2-9], including the time and space resolved accelerating electric field, the insulating magnetic field, the electron and ion temperatures and densities, and the plasma composition. Our goal is to apply similar techniques in the challenging PBFA II environment.

Descriptions of the PBFA II accelerator and the applied-B ion diode are given in References 13-15. This diode is sometimes refered to as a "barrel diode" because the anode is barrel shaped, with ions accelerated radially inward from the anode surface toward the center (see Figure 1). The virtual cathode is formed from a cloud of electrons which stream into the diode from the magnetically-insulated transmission lines, which supply the power. Electrons are

prevented from crossing to the anode by a magnetic field, which is applied parallel to the anode. This field is initially about 3 T but, due to diamagnetic effects[16], it rises to 5-10 T during the pulse. The peak voltage in present experiments is about 8 MV, with extracted ion currents of about 4 MA. More than 800 kJ has been coupled to an ion diode load. Hydrocarbon flashover anodes result in a proton beam which deposits, during a 20 nsec pulse, 50-75 kJ/cm^2 into a target with a 1 cm diameter focal spot. The best irradiance thus far obtained was 5.4 TW/cm^2 onto a 6mm diameter equivelant sphere. Present experiments use hydrocarbon flashover anodes to explore diode and target physics while other anodes are being developed for production of a lithium beam.

The plasmas which exist in this diode are both unique and complex, with expected electric fields of 10 MV/cm, magnetic fields of 5-10 T, and spatially and temporally varying plasma densities, temperatures, and composition. Thus, there are rich possibilities for spectroscopic investigations. However, the environment which exists on PBFA II is extremely harsh. Collection optics are bathed in a bremsstrahlung background with an 8 MeV endpoint energy, a typical dose 50 cm from the diode of 100 Rad(Si), and a dose rate of greater than 10^{10} Rad(Si)/sec. When the electrical power pulse arrives at the diode there are losses which result in electromagnetic pulse noise, making the operation of sophisticated electro-optic instruments difficult. The

first-surface optic of our spectroscopy system is routinely destoyed by debris on every shot. Finally, any instrumentation placed near the diode must be sufficiently robust that it can withstand the mechanical stresses induced when 30 TW of electrical power are deposited in the diode.

II. Instrument

The PBFA II visible spectroscopy system has been designed to maximize the data obtained in each shot, with a goal of obtaining a complete data set from a single shot. This is necessary because the shot rate is limited by induced radioactivity and hardware damage to roughly one per day, and it is expensive to repeat shots owing to the multiplicity of experiments scheduled for the large-scale PBFA II facility. A schematic for this system is shown in Figure 1. Light is collected from the anode region using collecting optics which consist of a mirror, a window and a 16 mm focal length, 12 mm diameter lens. The optics are housed in a manipulator which provides the capability for observing emission from varying distances away from the anode surface. The light is coupled into a 44 m long fiber optic link which transports the light to a remote screen room for recording. There, the light is injected into a 1 m f/7 Czerny-Turner spectrograph (S.I. McPherson, Inc.). An EG&G AVO model streak camera[17] is located at the exit focal plane of the spectrograph. This streak camera has a 40 mm long photocathode, a magnification of one, and a

microchannel plate (MCP) intensifier at the exit. Data is recorded on Kodak TMAX 400 film. At present we employ up to three streaked spectrograph systems to obtain data ion a single shot.

The spatial resolution of the streak camera is limited by the MCP to approximately 100 μm. With a 300 g/mm grating, the dispersion of the spectropgraph is 33.3 Å/mm so that the spectral resolution is about 3.3 Å with a range of 1332 Å. Higher resolutions are possible with different gratings, at the expense of lower sensitivity and less range. The streak camera was usually operated at its slowest sweep rate (400 nsec full sweep) with a temporal resolution of about 1 nsec. Convolved with the 22 MHz-Km bandwidth of the step-index fiber, the total system time resolution is about 1.5 nsec.

Several different fiber optic configurations have been used. Initially, a 400 μm diameter fiber (Raychem) was used to collect light from a 6 mm diameter, nearly cylindrical, region in the A-K gap. The distance between the collecting lens and the the diode midplane is fixed by the diode hardware to be about 26 cm. The maximum distance between the lens and the fiber is fixed because the lens diameter cannot be increased beyond 12 mm without interferring with other diagnostics and we need to ensure that the solid angle accepted by the fiber is filled with light. Therefore, the geometry of the collecting optics is determined and the

spatial resolution can only be improved by reducing the fiber diameter.

The second fiber configuration used was a linear array of ten 100 μm diameter fibers, with each fiber collecting light from a nearly cylindrical 2 mm diameter region in the A-K gap. An array was used instead of a single fiber in order to collect as much light as possible. The number of fibers which can be easily coupled into each system is limited to three by the 400 μm wide streak camera slit. Thus, a single ten-fiber array was capable of servicing three different spectrographs, each operating in a different spectral regime. The 3rd fiber optic configuration used was a 2x3 array of 100 μm fibers, allowing two systems to collect light from the same azimuthal location but at different distances from the anode surface.

An absolute timing fiducial was created for each system by placing a small cylinder of fast plastic scintillator (BC-418, Bicron Corp.) near the diode. When the power pulse arrives at the diode, electron losses generate a burst of high energy bremsstrahlung which floods the diode area. This bremsstrahlung creates light in the scintillator and the light is transported to the streak camera via a seperate fiber optic. By measuring the time difference between the arrival of the spectral signal compared to the scintillator and by using the timing of an electrically recorded (PIN diode) measurement of the x-ray pulse, we can relate the timing of the spectrum to any of the electically recorded

signals, including voltage, current, and beam intensity. The accuracy of this measurement is estimated to be +/- 3 nsec.

III. Calibrations

The efficiency with which light from the diode was collected into the fiber optic was measured by constructing a replica of the relevant diode hardware, including a segment of the cathode cone holding the collecting optic and its manipulator (Figure 2). A 100 μm fiber on an x-y-z translation stage, located at the equivelant position of the anode plasma, delivered light from a tungsten filament halogen lamp to the collecting optics system. A bandpass filter was used to select the wavelength. An absolutely-calibrated photodiode measures the output power of this source fiber and an absolutly-calibrated photomultiplier tube measures the light coupled into the PBFA II spectroscopy fiber, thus measuring the efficiency. Since the source fiber emits into a narrow cone, while light from the plasma is emitted into 4π, a correction of $NA^2/4$ is required, where NA is the source fiber numerical aperture. We measured the numerical aperture of the fiber and found that it agreed with the manufacturers specifications (0.22) to within +/- 5%. In addition, to prevent spurious signals due to propagation of cladding modes in the fiber, we used fiber manufactured by Raychem Corp. which has a buffer designed to eliminate these modes.

By translating the source fiber we were able to measure the absolute collection efficiency as a function of space (Figure 3). In actual operation the collecting lens is focused and aligned using a HeNe laser. The collection efficiency will vary depending on the actual wavelength region which is selected by the streaked spectrograph. Therefore, we also measured the collection efficiency as a function of wavelength, with the lens focus set using a HeNe laser in the same manner as on a PBFA II shot.

The transmission of the fiber optic link as a function of wavelength was measured using the setup depicted in Figure 4. Light from a mercury arc lamp was focused into a miniature monochromator (10 cm focal length, ISA Corp.). The monochromator bandwidth was 20 Å and the wavelength accuracy was +/- 2 Å. A 100 μm diameter Raychem fiber was connected to the exit of the monochromator and the power out of the end of this source-fiber was measured as a function of wavelength with an absolutely calibrated photodiode (position A, Figure 4). The source fiber was then connected to a 33.5 m coil of 200 μm diameter Raychem fiber (position B, Figure 4) and the power measurement was repeated with the photodiode at the end of the 200 μm fiber. The initial power measurement was then repeated in order to ensure that the light source was stable. Since the source fiber is smaller than the test fiber and the numerical apertures are the same, the difference in the two power measurements represents the fiber attenuation factor, except for about 4%

loss at the fiber interface. Excellent agreement was found between this data and the data supplied by the manufacturer. The attenuation for the fiber lengths used on PBFA II was approximately a factor of 82 at 3000 Å, 8.5 at 3500 Å, 3 at 4000 Å, and 2 at 7000 Å.

The sensitivity of the streaked spectrograph was measured with the same arc lamp/monochromator/fiber light source described in the fiber transmission measurement (Figure 4). The source fiber at the exit of the monochromator was first connected to the photodiode for calibration (position A, Figure 4), then it was connected to the fiber jumper at the input to the streaked spectrograph (position C, Figure 4). Fibers with 400 μm diameter provided enough light so that a single streak resulted in a detectable signal. Experiments performed with other fiber sizes at the spectrograph input require a correction factor. With the spectrograph grating set at a wavelength used in the PBFA II experiments, a series of streaks was taken, changing the wavelength selected by the monochromator between each streak. At the end of the streaked calibration we remeasured the light output from the source fiber to verify the stability of the light source. The film records of the streaks were digitized and the film response was unfolded. The absolute film response is determined for each streak record by placing a step wedge on the film using an absolutly calibrated sensitometer. Thus, we measure the

film exposure in erg/cm^2 for known values of the input power and input wavelength. Typical results are displayed in Figure 5. It is not certain at this time whether the structure in the sensitivity curve is due to a physical effect, such as variations in grating reflectivity or photocathode uniformity, or due to errors in the calibration. This measurement must be repeated for each grating used and for each grating wavelength setting. This process was time consuming and to date we have calibrated only two of the gratings used in these experiments. We are presently developing a more streamlined method for streaked spectrograph calibration.

This compilation of calibrations provides us with an absolute calibration for the entire streaked spectrograph system. We estimate that the system sensititvity is accurate to within a factor of two. As an example of the system sensitivity, if the plasma emits the Hα line (6563 Å) with a 10 Å linewidth and the system is set up with a 400 μm fiber, a 50 μm entrance slit, a 300 g/mm grating, a 400 nsec sweep, and 650 V on the MCP, then the power emitted by atoms in the plasma within our line of sight must exceed 1.2 W into 4π. This corresponds to about 5 μW or 0.5 μW/Å propagating in the fiber at the spectrograph entrance slit. For an 8 cm tall, 3 mm thick plasma, the plasma volume within our line of sight is 1.13 cm^3 and the required excited state population density is 1x10^{12} cm^{-3}.

IV. Fiber optic radiation effects

Two problems which can affect fiber optic systems in such a harsh radiation environment are Cerenkov light production and radiation-induced attenuation. In general, it is difficult to make accurate predictions of the effects of radiation on fiber optics. This is due to both a lack of fundemental understanding of the processes involved and the difficulty in measuring the spectrum, directionality and time-history of the radiation incident on the fiber. Therefore, it is desirable to directly measure the radiation effects under the same conditions as the actual experiment.

We first measured the Cerenkov light produced as a function of dose for Ensign-Bickford 200 μm diameter HCS fiber (NA = 0.37) on PBFA II shots with no large diagnostic shields in place to modify the background radiation. Absolutely-calibrated (+/- 18 %) photomultiplier tubes with bandpass filters were used. The filters had a center wavelength of 4000 Å and a bandwidth of 400 Å. The dose was measured by placing thermoluminescent detectors along the length of the fibers. We found that the Cerenkov light produced was linearly proportional to the product of dose and fiber length, as long as the exposure was low enough so that transient radiation-induced absorption in the fiber was not significant. The absolute Cerenkov light produced per unit exposure and per nanometer of wavelength interval was 3.1×10^{-17} J/(Rad(Si)-cm-nm) +/- 50%. This number is corrected for the attenuation in the fiber run located

outside the radiation environment which is used to transport the light to the screen room for recording. Pruett et.al.[18] performed a similar experiment exposing Raychem fiber (200 μm, NA =0.28) to a ^{60}Co source and obtained a value of 3.4×10^{-17} J/(R-cm-nm) at 5000 Å. The Cerenkov light coupled into the fiber is expected to scale as NA^2, λ^{-3}, and D^2, where D is the fiber diameter. When our result is scaled appropriately to correspond to the conditions in Reference 18, our value is 1.1×10^{-17} J/(Rad(Si)-cm-nm), a factor of three lower than the value given by Pruett et. al[18]. This discrepancy may be due to the difference in the radiation spectrum used, the difference between a pulsed and steady-state calibration, or to the material composition of the fibers. Finally, we performed additional measurements with 1mm diameter Ensign-Bickford fiber and found that the Cerenkov light coupled into the fiber does scale as D^2. Since this is the same scaling as for the signal, the signal-to-noise ratio is independent of the fiber diameter.

The highest exposures obtained in our tests were of order 50,000 Rad(Si)-cm. Based on the linear scaling of Cerenkov production with exposure in low-dose experiments, the Cerenkov light produced in high-dose experiments was a factor of 11 lower than expected. Assuming that this discepancy was due to radiation-induced attenuation, the inferred radiation-induced absorption coefficient was 12 dB/(m-kRad(Si)), with an estimated accuracy of a factor of 2. This is a factor of ten worse than the result obtained

for the same fiber exposed to high energy electrons from a Febetron source[19]. This result emphasizes the importance of performing experiments to test radiation effect under the same conditions which the fiber is intended to be used.

The durability of Raychem fiber jackets and low radiation-induced attenuation [20,21] prompted us to use Raychem fibers in our spectroscopy experiments. In our PBFA II experiments the exposure to the fibers is typically 5000-15000 Rad(Si)-cm, but the bremsstrahlung spectrum is modified by the presence of a 1000 kg tungsten shield which is used to protect other diagnostics. We measured the Cerenkov light by blanking off the ends of our fiber optics and recording the signal on the absolutely calibrated streaked spectrograph. We measured 2×10^{-18} J/(Rad(Si)-cm-nm) of Cerenkov light at 5800 Å and 9×10^{-18} J/(Rad(Si)-cm-nm) at 4250 Å. The estimated accuracy of +/- 50% may be responsible for the deviation from the expected λ^{-3} scaling. The difference between these results and the previous experiment with Ensign-Bickford fiber is probably due to the modifiction of the spectrum by the tungsten shield coupled with the fact that the energy dependence of the TLD response and the Cerenkov production in the fiber are different. The tungsten shield may reduce many of the photon energies below the approximately 200 keV required to produce Cerenkov light in the fiber, while essentially all the photons will be recorded by the TLD's.

We have not performed detailed measurements of the radiation-induced attenuation for the Raychem fiber used in these experiments. However, even if the induced attenuation were an order of magnitude higher than measured in Febetron experiments[20,21], the total induced loss would be less than 1 dB. Also, we compared the time-history of the Cerenkov light measured by the streaked spectrograph with the high-energy x-ray signal recorded with a PIN diode and found that they were identical. This implies that the radiation-induced attenuation is insignificant because the presence of induced attenuation is expected to modify the shape of the Cerenkov light pulse[22].

V. Results

The development of the streaked spectrograph system has enabled us to obtain spectra from three regions in the PBFA II diode: the plasma opening switch, the beam transport gas cell, and the anode plasma. An example of data from the anode plasma formed using a LiF flashover source is shown in Figure 6. Lineouts from the digitized spectrum at several times are shown in Figure 7. The lineouts are corrected for the film response but not the streaked spectrograph sensitivity. This data was obtained with the linear array of ten 100 μm diameter fibers aligned parallel to the anode, with each fiber collecting light from a nearly cylindrical 2 mm diameter region and the center of the line of sight located 2 mm from the anode surface. The anode was flat and

it was 8 cm tall. A 50 μm wide slit and a 300 g/mm grating centered at 6200 Å were used in the spectrograph. The streak camera used a 400 nsec sweep and 650 V on the MCP. The wavelength fiducials were applied by injecting a HeNe laser into the streaked spectrograph after the shot.

The Li I 2s-2p transition (6708 Å) in Figures 6 and 7 is blue-shifted early in time with the shift vanishing over about 10-15 nsec. The shift of the line center from the nominal wavelength is shown in Figure 8. We have interpreted this as a Stark shift due to the accelerating electric field across the diode gap. This interpretation is corroborated by the time-dependent intensity pattern of the Li I 2p-3d transition. This transition is split into two branches by the field with one branch blue-shifted and the other red-shifted. The components of the blue-shifted branch shift by up to 40 Å and the red-shifted branch shifts by 1.8 Å in a field of 1 MV/cm. In contrast, the 2s-2p line shifts by only 0.13 Å at 1 MV/cm. The large shifts for the 2p-3d transition compared to the 2s-2p line, and the large, rapid, changes in the electric field, make the 2p-3d emission difficult to observe early in time. The 2p-3d transition is only observed after almost all of the 2s-2p shift has vanished. When it first appears, the 2p-3d transition is split into two branches, as expected. We presently calculate[23] the Stark patterns for the lines neglecting the magnetic field. Using the 2s-2p shift given in Figure 8, this calculation yields peak electric fields of

7-8 MV/cm, the highest electric field ever measured using spectroscopic techniques.

VI. Conclusions

A streaked spectrograph system suited for operation in the harsh environment of PBFA II has been developed and calibrated. As with any complex diagnostic, this development process is evolutionary, and we are still seeking improvements. One important improvement is better capability in the ultraviolet. We are presently limited by the quartz fiber optic transmission to wavelengths longer than about 3000 Å. Shortening the fiber length should alleviate this problem but it will be necessary to locate the streak camera in the harsh radiation enviroment near the center of the accelerator.

We are presently constructing a model for the diode physics which is compatible with our spectroscopic observations. The observation of the electric field early in the pulse in a neutral lithium region provides information about the formation of the plasma. Such a neutral cloud has been suggested in previous work[5,24], but this is the first direct observation. We believe that the anode plasma forms by ionization of this neutral cloud. The time dependence of the Stark shift gives the ionization time of the neutral layer. The effective velocity of the ionization front is estimated to be 10 cm/μsec by dividing the line of sight diameter by the ionization time scale.

The development of a complete model for the behavior of applied-B ion diodes will require integration of such detailed spectrsoscopic observations with measurements of the properties of the extracted beam.

Acknowledgements

We are grateful to EG&G Energy Measurements Inc.for the loan of the streak cameras used in these experiments. We would also like to acknowledge the assistance with streak camera operations provided by R. Olsen (EG&G AVO) and R.W. Woodstra (EG&G KO). These experiments would not have been possible without the help of the dedicated PBFA II operations crew and the diode development team. We particularly thank D.J. Johnson, T.R. Lockner, K. Galvan, P. Lake, B. Morris, and P. Sawyer.

References

1. R. Pal and D. Hammer, Phys. Rev. Lett. 50, 732 (1983).

2. Y. Maron, M. Coleman, D.A. Hammer, and H.S. Peng, J. Appl. Phys. 61, 4781 (1987).

3. Y. Maron, M. Coleman, D.A. Hammer, and H.S. Peng, Phys. Rev. A 36, 2818 (1987).

4. Y. Maron, IEEE Trans. Plasma Sci. PS-15, 571 (1987).

5. C. Litwin and Y. Maron, Phys. Fluids B 1, 670 (1989).

6. Y. Maron, E. Sarid, O. Zahavi, L. Perelmutter, M. Sarfaty, Phys. Rev. A 39, 5842 (1989).

7. Y. Maron, E. Sarid, E. Nahshoni, O. Zahavi, Phys. Rev. A 39, 5856 (1989).

8. Y. Maron, M. Sarfaty, L. Perelmutter, O. Zahavi, M.E. Foord, and E. Sarid, Phys Rev. A 40, 3240 (1989).

9. Y. Maron, L. Perelmutter, E. Sarid, M.E. Foord, and M. Sarfaty, Phys. Rev. A 41, 1074 (1990).

10. H. Yoneda, T. Urata, K. Ohbayashi, Y. Kim, K. Horioka, K. Kasuya, Proc. IEEE Int. Conf. Plasma Sci., P. 100 (1987).

11. K. Masugata, H. Isobe, Y. Kawano, H. Venaga, W. Jiang, and K. Yatsui, Proc. 7^{th} Int. Conf. on High-Power Particle Beams, V. 1, p. 552 (1988).

12. Y. Kawano, N. Yumino, K. Masugata, and K. Yatsui, Laser Part. Beams 7, 277 (1989).

13. J.P. VanDevender and D.L. Cook, Science 232, 831 (1986).

14. D.L. Cook et. al., Plasma Phys. and Controlled Fusion 28, 1921 (1986).

15. D.J. Johnson et. al., Proc. 7th IEEE Pulsed Power Conf., Monterey, CA., p. 944 (1989).

16. S.A. Slutz, D.B. Seidel, and R.S. Coats, J. Appl. Phys. 59, 11 (1986).

17. R.W. Olsen, SPIE V. 981, p. 71 (1988).

18. B.L. Pruett, R.T. Peterson, D.E. Smith, L.D. Looney, and R.N. Shelton, Jr., SPIE V. 506, p. 10 (1984).

19. B.J. Skutnik and R.E. Hille, SPIE V. 506, p.184 (1984).

20. A.A. Hopkins, R.E. Kelly, L.D. Looney, and D.B. Lyons, SPIE V. 506, p.209 (1984).

21. D.E. Smith, D.R. Jander, F. Roeske, SPIE V. 721, p. 77 (1986).

22. W. Schneider, U. Babst, O.A. Balk, and E. Hochhauser, SPIE 506, p.189 (1984).

23. I.I. Sobelman, Atomic Spectra and Radiative Transitions, Springer-Verlag, New York (1979).

24. T.D. Pointon, J. Appl. Phys. 66, 2879 (1989).

Figure Captions

1. Schematic diagram of the PBFA II ion diode and the visible spectroscopy diagnostic. The diode is cylindrically symmetric about the indicated axis. The manipulator which houses the collecting optics is not shown.

2. Calibration geometry used for collection efficiency. The source fiber was mounted on an x-y-z translation stage which is not shown. The dashed line indicates the anode location on PBFA II (the anode was not present in the calibration). The manipulator for the collecting optics is not shown.

3. Collection efficiency as a function of distance away from the anode surface. The collecting optics were focused at 6328 Å and the measurement was made at 6500 Å. The correction for the source fiber numerical aperture is included.

4. Schematic diagram of the setup used to measure fiber transimission and the absolute streaked spectrograph sensitivity. The source fiber is connected to points A, B, or C, depending on whether we want to measure the source fiber output, the fiber transmission, or the streaked spectrograph sensitivity, respectively.

5. Streaked spectrograph sensitivity as a function of wavelength. The grating was tuned to a center wavelength of 6040 A.

6. Streaked spectrum from a PBFA II shot with a LiF anode. The timing fiducial is blooming because of insufficient

attenuation. The λ Fidu lines are wavelength calibration streaks applied with a HeNe laser after the shot. The LiI 2s-2p line begins at about the same time as the ion beam current.

7. Digitized lineouts as a function of time from the spectrum shown in Figure 6. The intensity has been corrected for the film response.

8. Shift of the LiI 2s-2p line-center wavelength as a function of time.

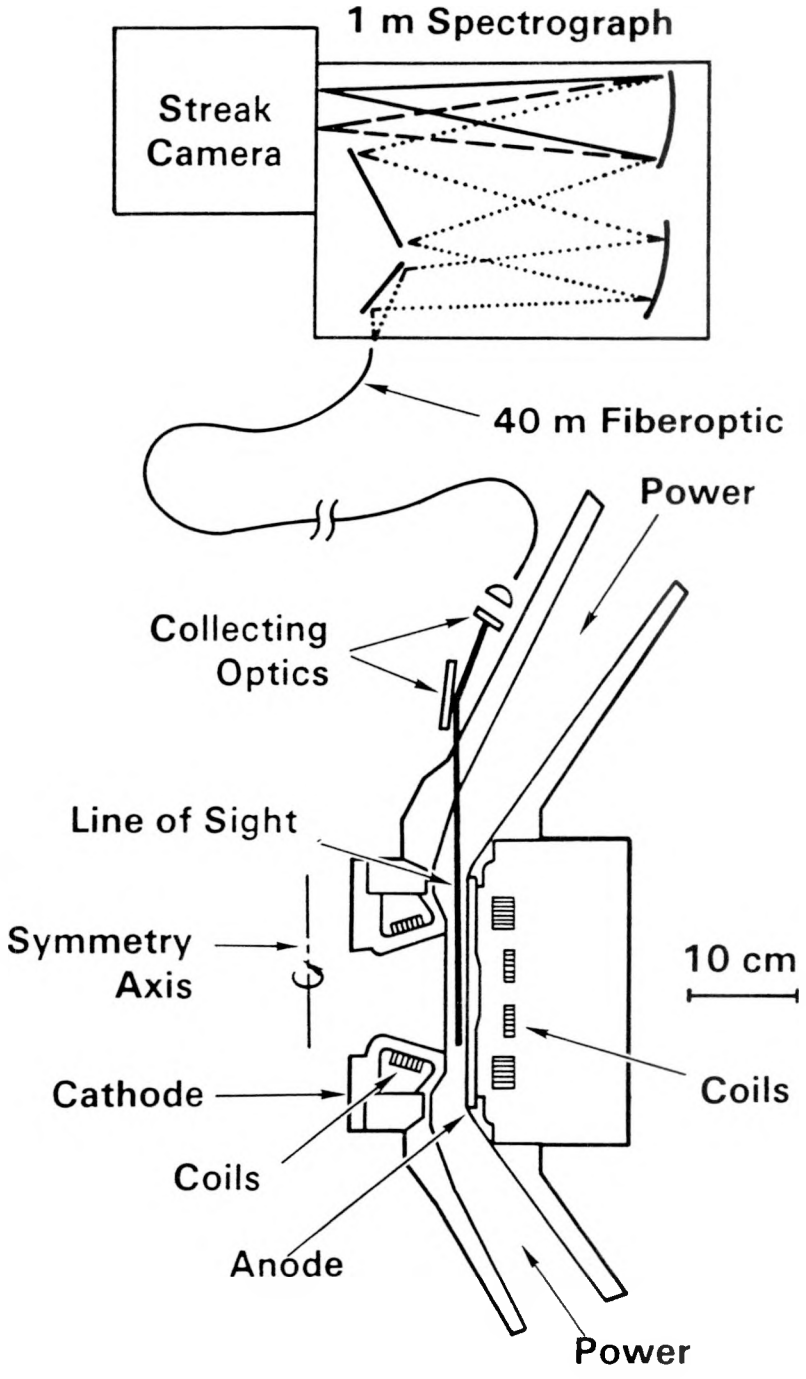

Figure 1 Bailey et al

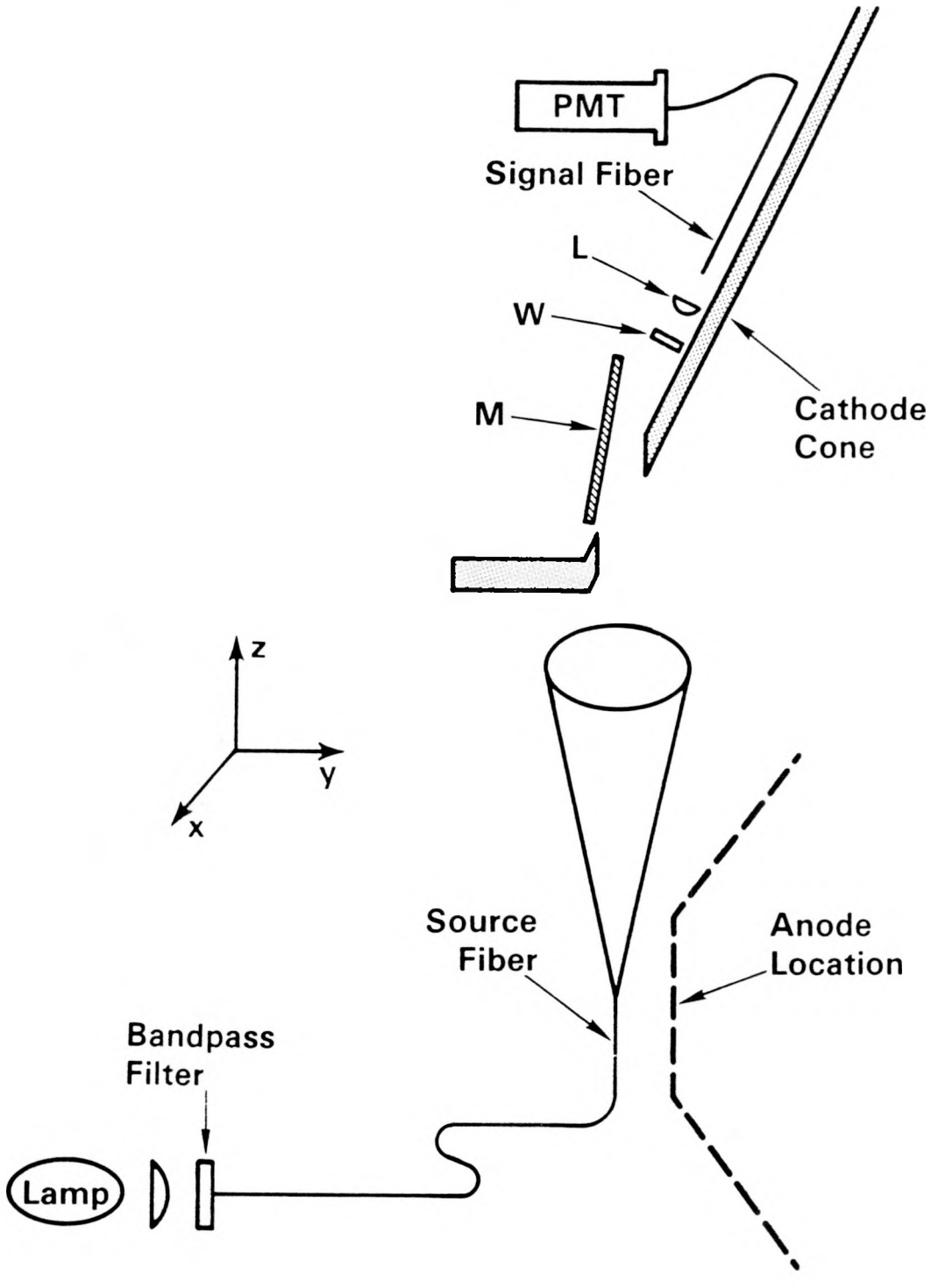

Figure 2 Bailey et al

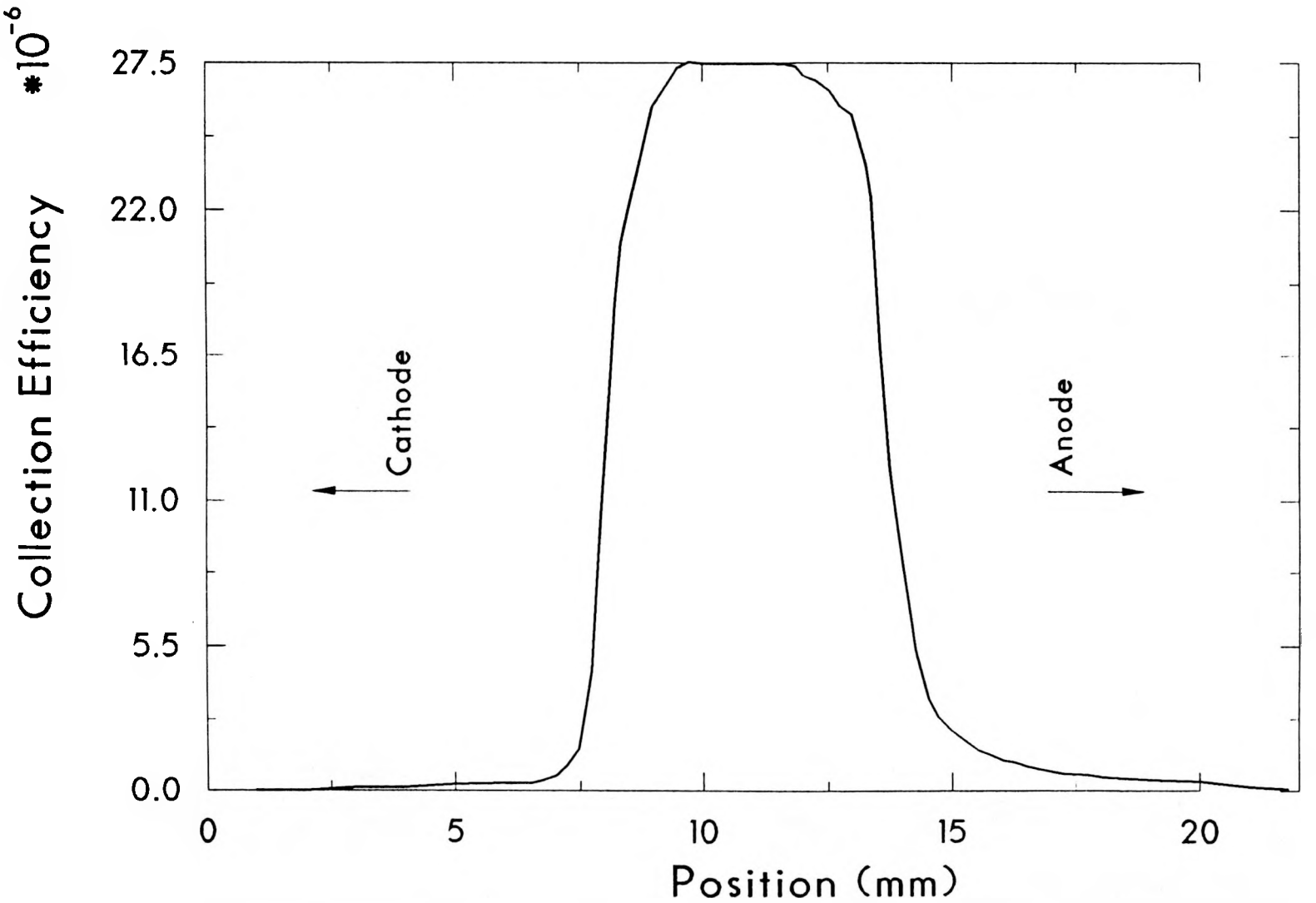
Collection Efficiency *10^-6
27.5
22.0
16.5
11.0
5.5
0.0
0
5
10
15
20
Position (mm)
Cathode
Anode

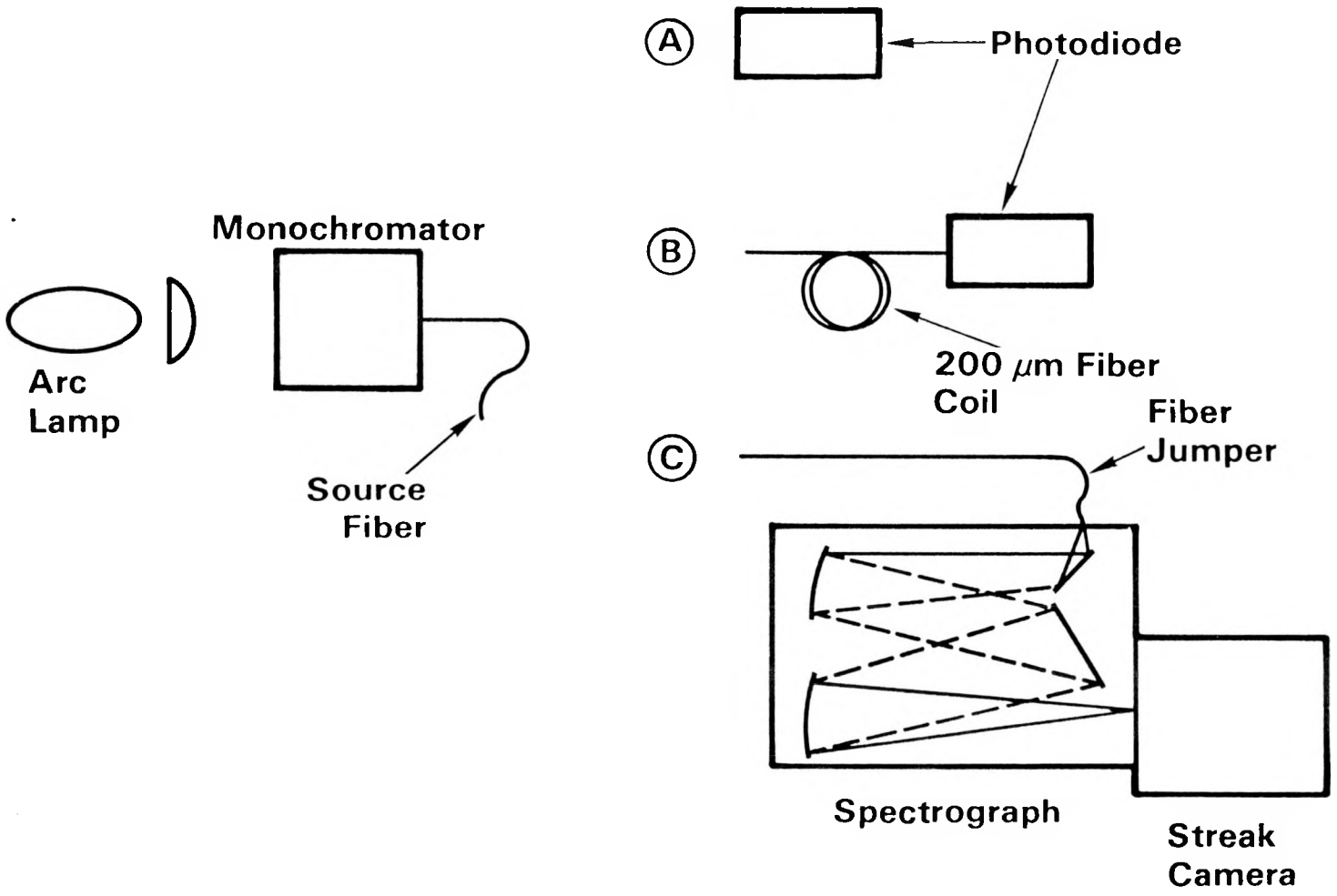
Monochromator
Arc
Lamp
Source
Fiber
A
Photodiode
B
200 μm Fiber
Coil
C
Fiber
Jumper
Spectrograph
Streak
Camera

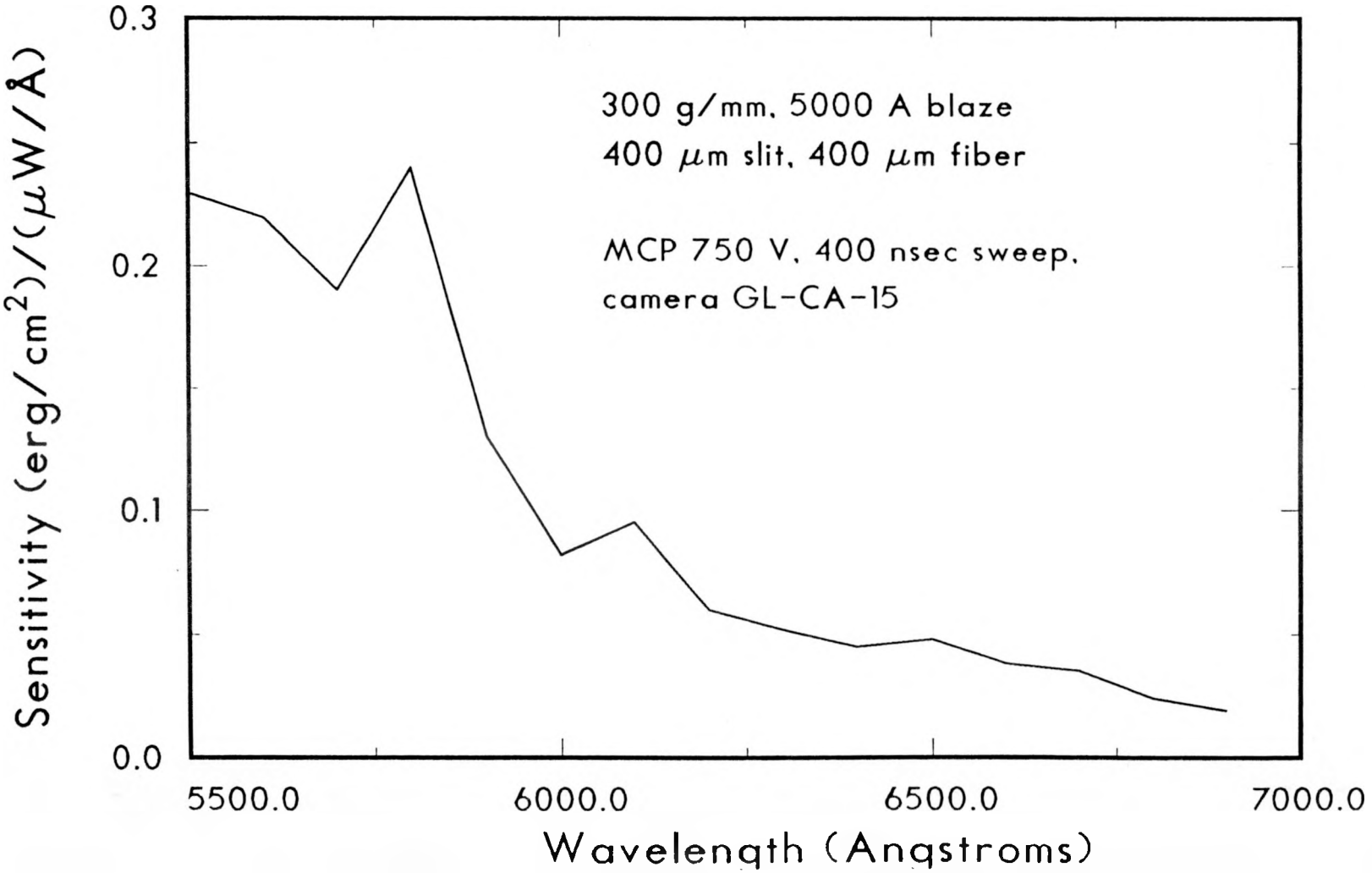
300 g/mm, 5000 A blaze
400 μm slit, 400 μm fiber
MCP 750 V, 400 nsec sweep,
camera GL-CA-15
Sensitivity (erg/cm²)/(μW/Å)
0.3
0.2
0.1
0.0
5500.0
6000.0
6500.0
7000.0
Wavelength (Angstroms)

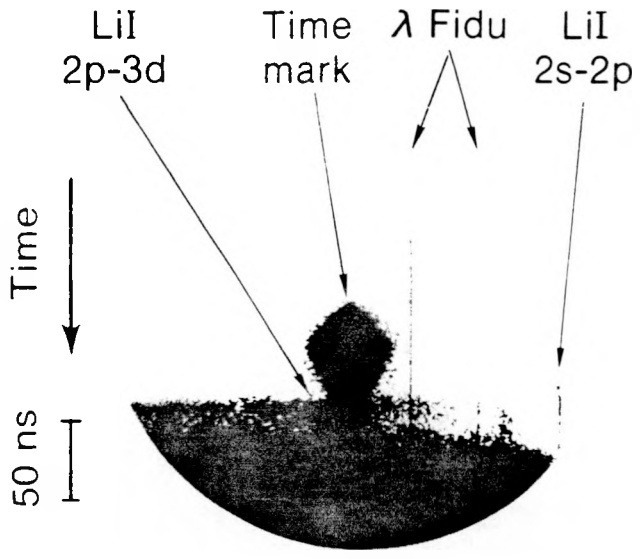
LiI
2p-3d
Time
mark
λ Fidu
LiI
2s-2p
Time
50 ns

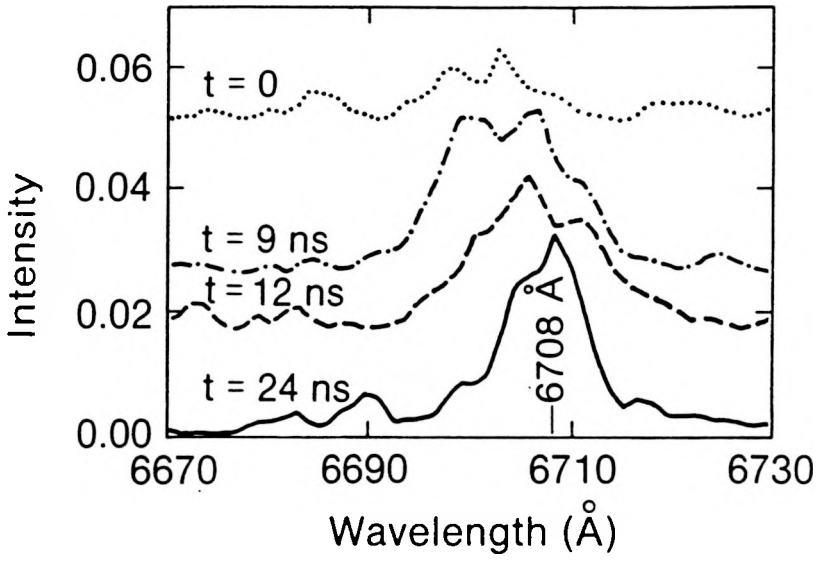

Figure 7 Bailey et al

Figure 8 Barley et al. 91